A Paleozoic age for the Tunnunik impact structure

Camille Lepaulard[1], Jérôme Gattacceca[1], Nicholas Swanson-Hysell[2], Yoann Quesnel[1], François Demory[1] , Gordon Osinski[3,4],

[1]Aix Marseille Univ, CNRS, IRD, Coll France, INRA, CEREGE, Aix-en-Provence, France

[2] Department of Earth and Planetary Science, University of California, Berkeley, California 94720-4767, USA

[3] Dept. of Earth Sciences, Centre for Planetary Science and Exploration, University of Western Ontario, 1151 Richmond St., London, ON, N6A 5B7, Canada

[4] Dept. Physics & Astronomy, University of Western Ontario, 1151 Richmond St., London, ON, N6A 5B7, Canada

Corresponding author: Camille Lepaulard (lepaulard@cerege.fr)

Key Points:

- The Tunnunik impact structure is most likely to have formed in the Late Ordovician to early Silurian
- The post-impact temperature of the studied target sedimentary rocks was about 350°C

This article was published as:
Lepaulard, C. Gattacceca, J., Swanson-Hysell, N.L., Quesnel, Y., Osinski, G. and Demory, F. (2019), A Paleozoic age for the Tunnunik impact structure, Meteoritics and Planetary Science, doi:10.1111/maps.13239

https://doi.org/10.1111/maps.13239

Abstract

We report paleomagnetic directions from the target rocks of the Tunnunik impact structure, as well as from lithic impact breccia dikes that formed during the impact event. The target sedimentary rocks have been remagnetized after impact-related tilting during a reverse polarity interval. Their magnetization is unblocked up to 350°C. The diabase dikes intruding these sediments retained their original magnetization which unblocks above 400°C. The impact breccia records a paleomagnetic direction similar to that of the overprints in the target sedimentary rocks. The comparison of the resulting virtual geomagnetic pole for the Tunnunik impact structure with the apparent polar wander path for Laurentia combined with biostratigraphic constraints from the target sedimentary rocks is most consistent with an impact age in the Late Ordovician or Silurian, around 430 to 450 Ma, soon after the deposition of the youngest impacted sedimentary rocks. Our results from the overprinted sedimentary rocks and diabase dikes imply that the post-impact temperature of the studied rocks was about 350°C.

1 Introduction

Hypervelocity impacts are a major process for the evolution of planetary surfaces, including the Earth. Terrestrial impact events have significantly influenced the biosphere in numerous ways including, on one hand, the development of habitats for primitive life forms (*Reimold and Koeberl*, 2008*; Cockell et al., 2005*) and, on the other hand, some extinctions such as the Cretaceous-Paleogene mass extinction (*Schulte et al*., 2010). Depending on the size of the impactor, impact events significantly modify regional geology and may lead to the formation of ore deposits (*Ames et al*., 1998). However, on Earth, plate tectonics and erosion can obscure or completely erase the geologic record of impact structures. Currently, around 190 impact structures are identified on Earth, including thirty in Canada, but the age of approximately half of these impacts is unknown (*Jourdan et al*., 2012). Dating of impact structures is crucial for assessing correlations (or the lack thereof) between impact events and biological or geological changes, and to constrain the flux of crater-forming bodies to the Earth through time.

While most of the large terrestrial impact structures (> 6 km) on Earth have likely already been documented (*Hergarten and Kenkmann*, 2015), discovery of additional impact structures is still possible. In 2010, the Tunnunik structure, a ~28 km diameter impact structure was identified in the Canadian Arctic (*Dewing et al*., 2013). The age of this structure is presently not constrained more precisely than between 0 and *ca*. 450 Ma. The purpose of this study is to provide a refined estimate for the age of this impact structure. In the absence of suitable material for radiometric dating, we utilize paleomagnetic dating of target rocks that were remagnetized by the impact (*Deutsch and Schärer, 1994; Pilkington and Grieve, 1992*) and of the lithic breccia that formed during the impact event (*Fairchild et al., 2015*).

2 Geological setting, sampling, methods

Geological setting

The Tunnunik impact structure is located on Victoria Island in the Canadian High Arctic. The impact structure is deeply eroded and has been identified by the presence of shatter cones, sedimentary rocks steeply dipping quaquaversally (compared to the generally relatively flat regional bedding), and concentric faults (*Dewing et al*., 2013). The target rock sequence, exposed outside of the impact structure, consists of sub-horizontal sedimentary rocks, mostly dolostones

and mudstones, ranging from the Neoproterozoic (Wynniatt formation of the Shaler supergroup) to the Late Ordovician - Early Silurian (?) (Thumb Mountain and Allen Bay formations). Following Newman and Osinski (2016), we group these sedimentary rocks into the Shaler Supergroup (Neoproterozoic), Mount Phayre, Victoria Island, Thumb Mountain and Allen Bay formations in ascending stratigraphic order.

Neoproterozoic diabase dikes associated with the *ca*. 720 Ma Franklin Large Igneous Province which intrude the Neoproterozoic sedimentary rocks are also present within the target rock (*Dewing et al*., 2013*; Heaman et al. 1992*). Lithic impact breccias, composed of sedimentary clasts up to centimeter size set in a silt-sized matrix, are encountered in the form of dikes and sills up to a few decimeters thick intruding the sedimentary target rocks, especially the Mount Phayre Formation and Shaler Supergroup rocks.

Sampling

Three main rock types were sampled for paleomagnetic analysis: impact breccia, Neoproterozoic to Upper Ordovician-lower Silurian sedimentary rocks, and Neoproterozoic diabase dikes. For impact breccia sampling, we focused on facies dominated by the fine-grained matrix (clast content below 10 vol%) and with clast size below 1 mm. A total of 29 paleomagnetic sites were sampled, mostly located inside the impact structure (Figure 1, Table S1). Sampling was performed by drilling of 2.5 cm-diameter cores using a gas-powered drill, or more rarely through collection of oriented blocks. Samples were oriented using magnetic and sun compasses.

Methods

The magnetic mineralogy was studied by measurement of susceptibility versus temperature (Figure 2A), stepwise thermal demagnetization of saturation isothermal remanent magnetization (sIRM) that is more sensitive to the presence of pyrrhotite (Figure 2B), and measurements of S_{-300} ratio that is the IRM obtained after applying a 3 T field and then a back field of − 0.3 T normalized to the IRM acquired in 3 T. The low field magnetic susceptibility

(noted χ in $m^3.kg^{-1}$) was measured for all samples using an AGICO apparatus, either with an MFK1 or a KLY-2 kappabridge instrument (with sensitivity of $5x10^{-13}$ m^3), depending on sample size. The MFK1 kappabridge operates at 200 Am^{-1} peak field and at a frequency of 976 Hz. The KLY-2 kappabridge operates at 425 Am^{-1} peak field and at a frequency of 920 Hz. Thermomagnetic curves were obtained with the use of the MFK1 instrument coupled with a CS3 furnace. Estimates of Curie temperatures were computed as the inflection points of the susceptibility versus temperature curves. Thermal demagnetization of sIRM (imparted with 3 T pulse with a MMPM9 pulse magnetizer) was conducted using an MMTD furnace. Hysteresis properties of the diabase dikes were measured with a MicroMag 3900 vibrating sample magnetometer. All rock magnetism measurements were performed at CEREGE.

All remanence measurements were performed with a SQUID magnetometer (2G Enterprises, model 760R, with noise level of 10^{-11} Am^2) in a magnetically shielded room, with an attached automated 3-axis alternating field degausser system (with a maximum peak field of 170 mT). For the majority of samples, the natural remanence was studied (around 100 specimens) by stepwise thermal demagnetization using a MMTD80 furnace. For each studied site, two pilot samples were demagnetized, one using thermal demagnetization up to 600°C, one using alternating field (AF) demagnetization up to 120 mT. The most efficient demagnetization method was then used for the remaining samples. Demagnetization data were analyzed through

principal component analysis and summarized with Fisher statistics using PaleoMac software (*Cogné*, 2003). Paleomagnetic results are summarized in Table 1.

3 Results

In the impact breccia, thermomagnetic experiments reveal a Curie temperature of 585°C, indicating the presence of magnetite (Figure 2A). Pyrrhotite is also present as indicated by significant unblocking of sIRM around 280-320°C (Figure 2B), although its signal is hidden by the magnetite contribution in the susceptibility curve (Figure 2A). The presence of pyrrhotite is confirmed by the S_{-300} ratio of -0.84 that indicates the significant contribution of a high coercivity mineral. The impact breccia samples display two magnetization components that are equally evidenced by thermal (Figure 3A) and AF demagnetization (Figure 3B). The low-temperature/low-coercivity component corresponds to the present local field. The high-temperature (isolated above ~200-350°C and up to the Curie temperature of magnetite at 585°C), high-coercivity (above 15 mT) component is origin-trending and is interpreted as the characteristic remanent magnetization (ChRM).

In the diabase dikes, the Curie temperature of ~570°C indicates the presence of magnetite, with a contribution of maghemite identified by an irreversible decay at around 350°C (Figure 2A). The diabase displays two components of magnetization, better evidenced by thermal (Figure 3C) than by AF demagnetization (Figure 3D). The high-temperature component, which is origin-trending, is unblocked between 400 and 590°C.

The magnetic mineralogy of rocks from Victoria Island and Shaler Supergroup is a mixture of pyrrhotite and magnetite. Pyrrhotite is evidenced by significant unblocking temperatures of sIRM around 300-320°C (Figure 2B), and the S_{-300} ratio of -0.79 that indicates the significant contribution of a high coercivity mineral. Pyrrhotite has previously been reported for the Cambrian-Ordovician sedimentary sequence in the region (e.g., *Quesnel et al*., 2013). The absence of field-dependence of low field magnetic susceptibility suggests a small pyrrhotite grain size (*Worm et al., 1993*), as classically found in many pyrrhotite-bearing sedimentary rocks (e.g., *Rochette et al., 1992*). Magnetite is indicated by the significant fraction of the sIRM unblocked above 330°C and up to 580°C (Figure 2B). Among the sedimentary rocks studied for paleomagnetism, 16 out of 21 sites showed unstable remanence during demagnetization and did not provide interpretable results, except for four sites from the Shaler Supergroup and for one site from the Victoria Island formation. These seven sedimentary rocks (dolostones and mudstones) display two components of magnetization, evidenced by thermal demagnetization (Figure 3E-F) where AF demagnetization (not shown) fails to separate both components. The origin-trending high-temperature component is unblocked between 290 and 350 °C (310°C for the only successful Victoria Island site, the remanence being too weak above this demagnetization step).

4 Discussion

It is crucial to determine the age of the remanent magnetizations identified in these rocks relative to the impact. The breccia dikes were formed during the impact event and their magnetic remanence would have been acquired both by the clasts and the fine-grained matrix as they cooled following emplacement and associated frictional heating. It has been shown that impact-

related tilting occurs quite rapidly, taking place over a timescale shorter than several minutes in mid-sized impact craters (*Fairchild et al*., 2016). Therefore, the impact breccia is expected to carry a thermoremanent magnetization acquired when the breccia cooled following impact-related tilting. Such a timing of impact acquisition has been shown for clastic breccia dikes within the Slate Island impact structure (*Fairchild et al*., 2016). However, because frictional heating in the breccia dikes is very localized *(Fairchild et al., 2016)*, the target sedimentary rocks and the diabase dikes may or may not have been remagnetized by the impact.

A paleomagnetic tilt test was used to estimate the relative timing of magnetization and impact tilting (*Tauxe and Watson,* 1994). This test was performed at site levels and not within sites because bedding was almost constant at each individual site. As expected, for all studied lithologies, the low-coercivity / low-temperature components fail the tilt test and were therefore acquired following tilting of the beds. The direction corresponds to the present day local magnetic field such that it is interpreted to be a recent viscous overprint (Figure 4C). For the impact breccia, the tilt test is also negative for the high coercivity components and progressive tilt test indicate a maximum grouping of the directions at 0% untilting. The ChRM of the breccia is interpreted as a full thermoremanent magnetization (TRM) acquired as the breccia cooled shortly after breccia emplacement and impact tilting. For the Shaler Supergroup, the tilt test is also negative, as illustrated by the much larger scattering after tilt correction (Figure 4A-B). Only one site from the Victoria Island formation provided paleomagnetic results suitable for interpretation. The tilt-corrected paleomagnetic direction for this site is compatible with that from the Shaler Supergroup and we considered it as a post-tilting impact related magnetization as well. The possible processes to account for post-tilting remagnetization of these sedimentary rocks are thermal magnetization during cooling from impact-related heating, shock magnetization during pressure release immediately after passage of the impact shock wave, or chemical magnetization resulting from post-impact hydrothermal activity (e.g., *Zylberman et al*., 2017). Shock remanent magnetization is excluded as the source of the impact-related magnetization because the release of the shock wave occurs before tilting, so that a shock remanence would pass a tilt test. Both partial or total TRM from impact-related heating and chemical remanent magnetization (CRM) from impact-related hydrothermal activities can result in a remagnetization allowing the structure to be paleomagnetically dated (*Pilkington et al., 1992*). In view of the unblocking temperatures of the natural remanent magnetization (NRM) in the sedimentary rocks (290°C to 350°C), a CRM could be explained by the formation of pyrrhotite during hydrothermal activity (e.g., *Osinski et al., 2005*). However, because the maximum unblocking temperature of 350°C is slightly higher than the Curie temperature of pyrrhotite (320-325°C), we favor a partial thermoremanent magnetization acquired during post-impact cooling from a peak temperature of 350°C.

For the three diabase dikes, the tilt test is inconclusive because the beddings of the intruded sediments are similar for the three sites. The ChRM direction is significantly different (before tilt correction) to the average direction computed from the Shaler Supergroup, Victoria Island formation and impact breccia, suggesting that they have not been remagnetized by the impact (Figure 4B). Their virtual geomagnetic poles (VGPs, after tilt correction) are closer to paleomagnetic poles from other igneous rocks of the Franklin Large Igneous Province (*Palmer et al., 1983; Denyszyn et al. 2009*) than the impact breccia site VGPs. Poorly developed shatter cones have been described in the diabase dikes (*Dewing et al., 2013*), implying shock pressures above ~2 GPa during the impact event. Such pressure level is well below the pressure-induced magnetite magnetic transition at 12-16 GPa (*Ding et al., 2008*). Moreover, the coercivity of

remanence of samples from the diabase dikes is 39 mT (our measurements, average of 3 samples, one per studied dike), and significant shock remagnetization is also unlikely for magnetite with this range of coercivity of remanence (*Bezaeva et al., 2010*).

To test further whether or not the diabase dikes have preserved their primary TRM, we collected 4 oriented cores of the Shaler supergroup sedimentary rocks that were intruded and baked by the dike, at distances from 3 to 25 cm from the dike wall. In addition to a low temperature viscous component, these samples exhibit four magnetization components unblocked over the following temperature range: between 250 and 345°C, between 345 and 370, between 370 and 450°C, and above 450°C (Table 1, Figure 3G). These components are called A, B, C, D in the following for clarity. Among the three higher temperature components components B and D are identical and close to the reverse polarity ChRM of the diabase dikes (Figure 4C). Component C is antipodal to components B and D. These three components are interpreted as partial TRMs acquired successively during cooling from above 500°C following the diabase dike intrusion. During cooling, the geomagnetic field changed from reverse to normal and back to reverse polarity, leading to the record of antipodal directions D, C, and B successively. Such a record of successive polarity intervals has already been observed in slow cooling sedimentary rocks (e.g., *Rochette et al. 1992*). Component A blocked up to 345°C has a direction different from the other 3 components related to the dike intrusion but undiscernible (before tilt correction) from the other remagnetized Shaler Supergroup directions. It is interpreted as a partial TRM acquired following the impact. This result indicates that the post-impact temperature in these rocks was 345°C, in close agreement with the ChRM peak unblocking temperatures measured in the other Shaler Supergroup sediments within the impact structure. Component A is not recorded in the diabase dikes because these rocks have minimal blocking capacity below 350°C.

The impact breccia, Shaler Supergroup formation, and Victoria Island formation all have post-tilting impact-related ChRM. These seven paleomagnetic directions are similar (Figure 4B) and the mean pole calculated from these sites is: 349.3°E, 1.2°N, angular radius of 95% confidence cone A_{95} = 8.3°, and Fisher precision parameter K = 53.3 (Table 1). The sites may have slightly different magnetization ages due to different blocking temperatures and varied cooling history and as a result may partially average out secular variation. However, the conservative interpretation is that the combined pole represents a snapshot of the paleomagnetic field shortly following impact that does not average out secular variation and should be considered a virtual geomagnetic pole rather than a mean paleomagnetic pole.

Comparison of this impact pole with the running mean Apparent Polar Wander Path (APWP) for North America (*Torsvik et al*., 2012; *Besse and Courtillot,* 1991) shows that it is closest to the 520, 510 and 500 Ma mean paleomagnetic poles (Figure 5).

Following 500 Ma, the angular distance of the Tunnunik VGP becomes progressively greater from the geographic poles implied by the running mean poles of *Torsvik et al.* (2012) and the paleogeographic model of *Torsvik and Cocks* (2017) and its modification by *Swanson-Hysell* and *Macdonald* (2017) (Figure 6A). From 410 Ma onward to the present, the angular distance between the Tunnunik VGP and the geographic pole exceeds 45º. Deviations between the geographic pole and a virtual geomagnetic pole are expected to arise through secular variation of the geomagnetic field. However, secular variation of the geomagnetic field typically leads to geomagnetic pole positions that are close to the geographic pole. For example, random draws from the paleosecular variation model TK03.GAD (*Tauxe and Kent,* 2004) for a site at the equator will be within 20º of the geographic pole 90% of the time and within 30º of the

geographic pole 95% of the time. The further away an impact VGP is from a pole of a given age, the less likely it is to have formed at that age (see similar discussion in *Hervé et al*., 2015 and *Carporzen and Gilder*, 2006). In order to estimate the probability of the Tunnunik VGP having arisen through secular variation throughout the Phanerozoic, the approach developed by *Fairchild et al.* (2016) was used: the angular distance between the Tunnunik VGP and the paleopoles is compared to that of VGPs randomly sampled from the TK03.GAD secular variation model (*Tauxe and Kent,* 2004). For this analysis, we simulated 10^5 VGPs from the TK03.GAD model in 10 million year increments at the paleogeographic position of the crater. Seeking to quantify the probability of an angular deviation between the paleopole and the Tunnunik VGP as large as that determined at each of these times (Figure 6A), we calculated the percentage of simulated VGPs that are at this angular distance or greater from the pole (Figure 6B and 6C). While the Tunnunik VGP is closest to North America's pole path at *ca*. 500 Ma, this analysis shows that the likelihood of a VGP with the angular distance as large as the deviation of the paleopole of the Tunnunik VGP is greater than 5% at every simulated time during the Ordovician, using the minimum angle given the uncertainty of the VGP. However, given the increasing angular distance of the Tunnunik VGP from Silurian paleopoles (from 420 Ma onward), the likelihood of a VGP at such a distance is less than 5% and continues to be a low probability event all the way to the present. The magnetostratigraphy scale for the 500-420 Ma time interval (e.g., *Hounslow et al*., 2016), although incomplete, shows multiple reversals and does not allow to better constrain the age of the reverse polarity remagnetization observed at Tunnunik structure.

Geologic constraints on the timing of the impact come from the age of early Paleozoic shallow-marine sedimentary rocks within the Tunnunik impact structure. Extensive mapping of the shatter cone distribution at the impact structure reveal the youngest rocks with shatter cones to be those of the Victoria Island Formation (*Osinski and Ferrière*, 2016). Conodont biostratigraphy has revealed an Early Ordovician age (*ca*. 487 to 470 Ma) for the Victoria Island Formation (*Dewing et al*., 2013; *Dewing et al*., 2015). Faulting associated with impact crater development extends beyond the central region that contains shatter cones and deforms rocks of the Thumb Mountain Formation (*Dewing et al*., 2013; *Newman and Osinkski*, 2016). Conodonts and a fossil assemblage of crinoids, corals, gastropods, and cephalopods indicate a Late Ordovician age for the Thumb Mountain Formation (*ca*. 458 to 445 Ma; *Dewing et al*., 2013). Overlying the dolostone of the Thumb Mountain is a poorly exposed dolostone unit that Dewing et al. (2013) tentatively assigned to the Allen Bay Formation. Further to the northwest on the Arctic Platform at Devon Island, biostratigraphy on carbonates of the Allen Bay Formation have revealed it to have an age that spans from the Late Ordovician into the Silurian (*Thorsteinsson and Mayr*, 1987). Mapping of the impact structure has largely left rocks assigned to the Thumb Mountain and Allen Bay Formations undivided (*Dewing et al*., 2013; *Newman and Osinski*, 2016). Currently the most robust constraint on the maximum age of the impact event is that the development of the impact structure led to faulting of the Thumb Mountain Formation and therefore occurred after *ca*. 458 Ma. Regional normal faults taken to have formed in association with Early Cretaceous extension cut across the impact structure were interpreted to indicate that the crater formed before *ca*. 130 Ma (*Dewing et al*., 2013), but this constraint is rather speculative.

The position of the Tunnunik VGP is most consistent with an Ordovician age for the Tunnunik impact. While secular variation of the geomagnetic field naturally results in VGPs that differ from the mean paleopole position, the large angle between the Tunnunik VGP and

paleopoles 420 Ma and younger makes a deviation of this magnitude a low probability event (Figure 6). The combined paleomagnetic, stratigraphic and biostratigraphic constraints collectively suggest a Late Ordovician to Silurian age of ca. 430-450 Ma, only shortly after deposition of the youngest impacted sediments.

5 Conclusions

This study focuses on constraining the age of the recently discovered Tunnunik impact structure. Paleomagnetic directions obtained from impact breccia and sedimentary rocks from the target sequence indicate the acquisition of a magnetization following impact-related tilting during a reverse polarity interval. In contrast, the diabase dikes intruding these sediments have retained their original magnetization unblocked above 400ºC. The comparison of the resulting paleomagnetic pole with the apparent polar wander path for North America shows it to be close to Cambrian poles and strongly suggests a Paleozoic age for the crater. The likelihood of the observed impact direction becomes very small (<5% likelihood) if it was acquired after ca. 430 Ma suggesting an age of impact that is older than 430 Ma. Combined with the stratigraphic constraints these data indicate an impact age between 450 and 430 Ma, in the Late Ordovician or Silurian Period, soon after deposition of the youngest impacted sedimentary rocks. This old age opens the possibility that ejecta from the Tunnunik crater may have been preserved in the surrounding basin and may be found in the sedimentary rocks of the Arctic platform.

The target sedimentary rocks were remagnetized during post-impact cooling. The preservation of pre-impact magnetization unblocked above 400°C in the diabase dikes, and the constraints from the paleomagnetic results obtained on the Shaler Supergroup sediments baked by the intrusions of the diabase dikes indicate collectively that the peak temperature of the thermal excursion associated with the impact was 350°C at the structural level of the studied rocks.

Acknowledgments

This project was partly funded by the French Polar Institute IPEV (Institut Paul Emile Victor). The authors are grateful to the Polar Continental Shelf Project for logistical support. The France-Berkeley Fund initiated collaborative research between J.G. and N.L.S.-H. We thank William Zylberman, Cassandra Marion-Beauchamp, and Racel Sopoco for their help in the field during sampling.

References

Ames, D.E., Watkinson, D.H. and Parrish, R.R. (1998), Dating of a regional hydrothermal system induced by the 1850 Ma Sudbury impact event, Geology, 26, 447–450.

Besse, J. and V. Courtillot (1991), Revised and Synthetic apparent polar wander path of the African, Eurasian, North American and Indian plates, and True polar wander since 200 Ma, J. Geophys. Res., 96, 4029–4050.

Carpozen, L. and S.A. Gilder (2006), Evidence for coeval Late Triassic terrestrial impacts from the Rochechouart (France) meteorite impact, Geophysical research letters, v.33, L19308, doi: 10.1029/2006GL027356.

Cockell, C. S., Lee, P., Broady P., Lim, D., Osinski, G., Parnell, J., Koeberl, C., Pesonen, L., and Salminen, J., 2005. Effects of Asteroid and Comet Impacts on Lithophytic Habitats – A Synthesis. Meteoritics and Planetary Science, 40, 12, 1-14.

Cogné, J.P (2003), PaleoMac: A Macintosh™ application for treating paleomagnetic data and making plate reconstructions, Geochemistry, Geophysics, Geosystems, 4, 1, 1007, doi: 10.1029/2001GC000227.

Denyszyn, S. W., Halls, H. C., Davis, D. W., and Evans, D. A. (2009). Paleomagnetism and U–Pb geochronology of Franklin dykes in High Arctic Canada and Greenland: a revised age and paleomagnetic pole constraining block rotations in the Nares Strait region. *Canadian Journal of Earth Sciences*, *46*(9), 689-705.

Deutsch A., Schärer U. (1994) Dating terrestrial impact events. Meteoritics, 29, 301-322.

Dewing, K., Pratt, B.R., Hadlari, T., Brent, T., Bédard, J. and R.H.Rainbird (2013), Newly identified "Tunnunik" impact structure, Prince Albert Peninsula, northwestern Victoria Island, Arctic Canada, Meteoritics & Planetary Science, 48, 2, 211-223, doi: 10.1111/maps.12052.

Dewing, K., Hadlari, T., Rainbird, R.H., and Bédard, J.H., 2015. Phanerozoic geology, northwestern Victoria Island, Northwest Territories; Geological Survey of Canada, Canadian Geoscience Map 171 (preliminary), scale 1:500 000. doi:10.4095/295530

Ding Y., Haskel D., Ovchinnikov S. G., Tseng Y.-C., Orlov Y. S., Lang J. C., Mao H. (2008) Novel Pressure induced magnetic transition in magnetite (Fe3O4) Physical Review Letters, 100, 045508.

Fairchild, L.M., Swanson-Hysell, N.L. and S.M. Tikoo (2016), A matter of minutes: Breccia dike paleomagnetism provides evidences for rapid crater modification, Geological Society of America, 44, 9, 723-726, doi: 10.1130/G37927.1.

Gradstein, F.M., Ogg, J.G. and F.J. Hilgen (2012), On the Geological Time Scale, Newsletters on Stratigraphy. 45. 171-188., doi:10.1127/0078-0421/2012/0020.

Heaman L. M., LeCheminant A. N., and Rainbird R. H. 1992. Nature and timing of Franklin igneous events, Canada: Implications for a Late Proterozoic mantle plume and the break-up of Laurentia. Earth and Planetary Science Letters 109:117–131.

Hergarten, S. and T. Kenkmann (2015), The number of impact craters on Earth: any room for further discoveries ?, Earth and Planetary Science Letters, 425, 187-192.

Hervé, G., Gilder, S.A., Marion, C.L., Osinski, G.R., Pohl, A., Petersen, N. and P.J.Sylvester (2015), Paleomagnetic and rock magnetic study of the Mistastin Lake impact structure (Labrador, Canada): implications for geomagnetic perturbation and shock effects, Earth and Planetary Science Letters, 417, 151-163, doi:10.1016/j.epsl.2015.02.011.

Hounslow, M.W (2016), Geomagnetic reversal rates following Palaeozoic superchrons have a fast restart mechanism, Nature communication, doi: 10.1038/ncomms12507.

Jourdan, F., Reimold, W.U. and A. Deutsch (2012), Dating terrestrial impact structures, Elements, 8, 49-53, doi: 10.2113/gselements.8.1.49.

Newman, J.D. and G.R. Osinski (2016), Geological mapping of the Tunnunik impact structure, Victoria Island, Canadian High Arctic, paper presented at the 47th Lunar and Planetary Science Conference, Houston.

Osinski, G.R. and L. Ferrière (2016), Shatter cones: (Mis)understood?, Sciences advances, 2, 8, doi: 10.1126/sciadv.1600616.

Osinksi, G.R., Lee, P., Parneell J., Spray, J. G., Baron, M. (2005) A case study of impact-induced hyrothermal activity: the Haughton impact structure, Devon Island, Canadian High Arctic, Meteoritics & Planetary Science, 40, 1859–1877.

Palmer, H.C., Baragar, W.R.A., Fortier, M. and Foster, J.H. (1983), Paleomagnetism of Late Proterozoic rocks, Victoria Island, Northwest Territories, Canada, Canadian Journal of Earth Sciences, 20, 1456-1469, doi: 10.1139/e83-131.

Quesnel, Y., Gattacceca, J., Osinski, G.R. and P. Rochette (2013), Origin of the central magnetic anomaly at the Haughton impact structure, Canada, Earth and Planetary Science Letters, 367, 116-122.

Reimold, W.U. and C. Koeberl (2008), Catastrophes, extinctions and evolution: 50 years of impact cratering studies, Golden Jubilee Memoir of the Geological Society of India, 66, 69-110.

Schulte, P. and 40 co-authors (2010), The Chicxulub asteroid impact and mass extinction at the Cretaceous-Paleogene boundary. Science, 327, 1214-1218.

Sodero, D.E. and J.P.J. Hobson, (1979), Depositional Facies of Lower Paleozoic Allen Bay Carbonate Rocks and Contiguous Shelf and Basin Strata, Cornwallis and Griffith Islands, Northwest Territories, Canada. Am. Assoc. Pet. Geol. Bull., 63, 1059-1091.

Swanson-Hysell, N. L. and F. A. Macdonald (2017), Tropical weathering of the Tacnic orogeny as a driver for Ordovician cooling, Geology, doi:10.1130/G38985.1

Thorsteinsson, R. and U. Mayr. (1987), The sedimentary rocks of Devon Island, Canadian Arctic Archipelago, Geological Survey of Canada Memoir, 411, 182.

Tauxe, L. and D.V. Kent (2004). A simplified statistical model for the geomagnetic field and the detection of shallow bias in paleomagnetic inclinations: Was the ancient magnetic field dipolar? *In* J. Channell, D. Kent, W. Lowrie, & J. Meert (Eds.), Timescales of the Paleomagnetic Field, 145, 101–116. Washington, D.C.: AGU.

Tauxe, L. and G.S. Watson (1994), The fold test – an eigen analysis approach, Earth and Planetary Science Letters, 122, 331-341.

Torsvik, T.H. and L.R.M. Cocks (2017), Earth history and palaeogeography: Cambridge, UK, Cambridge University Press, 311, doi: 10 .1017/9781316225523.

Torsvik, T.H., Van Der Voo, R., Preeden, U., Mac Niocaill, C., Steinberger, B., Doubrovine, P.V., Van Hinsbergen, D.J.J., Domeier, M., Gaina, C., Tohver, E., Meert, J.G., McCausland, P.J.A. and L.R.M. Cocks (2012), Phanerozoic polar wander, palaeogeography and dynamics, Earth Science Reviews, 114, 325-368, doi: 10.1016/j.earscirev.2012.06.007.

Worm, H.-U., Clark, D., Dekkers, M.J. (1993) Magnetic susceptibility of pyrrhotite: grain size, field and frequency dependence. Geophys. J. Int., 114:127-137.

Zylberman, W., Quesnel, Y., Rochette, P., Osinski, G.R., Marion, C. and J. Gattacceca, (2017), Hydrothermally-enhanced magnetization at the center of the Haughton impact structure?, Meteoritics and Planetary Science, 1-19, doi:10.1111/maps.12917.

Figure and Table captions

Figure 1. Location of sampled sites. Color codes indicate the sampled formation. Numbered sites are the ones that provided interpretable paleomagnetic results. The red circle is the proposed limit of the impact structure from Newman and Osinski (2016). The purple contour delineates the area where shatter cones have been found. The background image is an Advanced Spaceborne Thermal Emission and Reflection Radiometer (ASTER) Global Digital Elevation Model (GDEM) Version 2 product. The elevation ranges from 0 (white) to 283 m (black). Except for the regional map on the upper left, coordinates are expressed in meters in the Universal Transverse Mercator (UTM) Zone 12 projection with the World Geodetic System

(WGS) 84 datum. For the zoomed-in area (upper right), the background image is to a mosaic of orthophotographic images (Digital Globe Quickbird data).

Figure 2. Intrinsic magnetic properties of studied rocks. A) Susceptibility versus temperature for a diabase dyke sample (site TUN32, heating and subsequent cooling curves are shown), and an impact breccia sample (site TUN20). B) Thermal demagnetization of sIRM as a function of temperature. The red box indicates the unblocking temperature range of the impact-related magnetization of the target sedimentary rocks. The blue box indicates the unblocking temperature range of the pre-impact magnetization of the diabase dikes. The post-impact temperature excursion is constrained between these two boxes. The Curie temperature of pyrrhotite (325°C) is indicated by the thick vertical line.

Figure 3. Orthogonal projection plot of stepwise demagnetization data before tilt-correction. Representative samples of the 3 main formations are presented: A-B) Lithic impact breccia, C-D**)** diabase dike, E**)** Shaler Supergroup, F) Victoria Island formation. G) Shaler Formation sample collected 25 cm away from the diabase dike of site TUN32. For clarity the four components of magnetization recorded in this sample and discussed in the text are highlighted by colored arrows.

Figure 4. Equal area stereographic projections. Open (closed) symbols are for upper (lower) hemisphere directions. **A)** Directions of the 24 samples from 4 sites of the Shaler Supergroup sediments before (left) and after (right) tilt correction. The red symbols are the low temperature components (isolated between 280 and 330°C) of the four samples collected within 25 cm of the diabase dike of site TUN32. Blue star is the overall mean direction (samples from site TUN32 not included). **B)** Low temperature directions (grey symbols) and ChRM directions for the seven sites from the impact breccia, Shaler Supergroup and Victoria Island Formation listed in Table 1, before tilt correction. Also shown is the average ChRM direction for the 3 diabase dikes (square), and the average present day magnetic field (red star). **C)** Directions of the four components of magnetization from the Shaler Supergroup sediments collected within 25 cm of the diabase dike at site TUN32. Also shown is the ChRM direction of the diabase dike at this site (in red).

Figure 5. Comparison of the running mean APWP of Laurentia (*Torsvik et al., 2012*) with the Tunnunik virtual paleomagnetic pole which is the average of the virtual geomagnetic poles of the impact breccia, Shaler Supergroup Formation and Victoria Formation sites. Ages of the running mean APWP poles are labeled from the Cambrian to the Early Devonian. The running mean poles are shown with the calculated 95% confidence circle (A95) associated with the mean of studies that fall within a 20 Myr sliding window. The poles for 520, 460, 450, 390, 380, 360 and 350 Ma are shown with no such confidence circle as there are no studies within the sliding window and the position of the pole for that age is the result of linear interpolation by *Torsvik et al. (2012)*.

Figure 6. A) Angle between Tunnunik impact VGP and paleopoles as a function of time for the *Torsvik et al.* (2012) APWP, the paleogeographic models of *Torsvik and Cocks* (2017) and its

Ordovician modification by *Swanson-Hysell and Macdonald* (2017). **B)** likelihood for a VGP to occur at an angular deviation from the paleopole equal or greater to that observed for the Tunnunik impact VGP for a Fisherian (k=20) distribution of VGPs. **C)** likelihood for a VGP to occur at an angular deviation from the paleopole equal or greater to that observed for the Tunnunik impact VGP for VGPs drawn from the TK03.GAD secular variation model.

Table 1. Site-mean paleomagnetic directions from the Tunnunik impact structure. Site TUN32# is for Shaler Supergroup sediments baked by the diabase dike at site TUN32. These samples have four components of magnetization (A, B, C, D, see text). S_{Lat} and S_{Long}, site latitude and longitude; N/n, number of samples used in the computation of the mean direction / number of samples stepwise demagnetized; ChRM unblocking temperature, the temperature interval of the high temperature component used for calculation; D_g and D_s, declination before and after tilt correction; I_g and I_s, inclination before and after tilt correction; k_g and k_s (noted Kg and Ks for the average of VGPs) precision parameter before and after tilt correction; α_{95}^g and α_{95}^s (noted A95g and A95s for the average of VGPs) are semi-angle of aperture of the cone where the true mean direction lies with 95% confidence before and after tilt correction; Strike, strike of the site; Dip, dip of the site; *, Strike and Dip range from 162/16 to 190/38 (site TUN20), from 213/60 to 193/70 (site TUN33); For impact breccia and diabase dikes sites, strike and dip are for the intruded rocks; dp is the semi-axis of the confidence ellipse about the VGP along the great circle path from site to VGP; dm is the semi-axis of the confidence ellipse perpendicular to that great-circle path. NRM, average natural remanent magnetization; χ, average magnetic susceptibility. *The average impact is computed from sites TUN07, 20, 21, 29, 31, 33, 36 (see text).

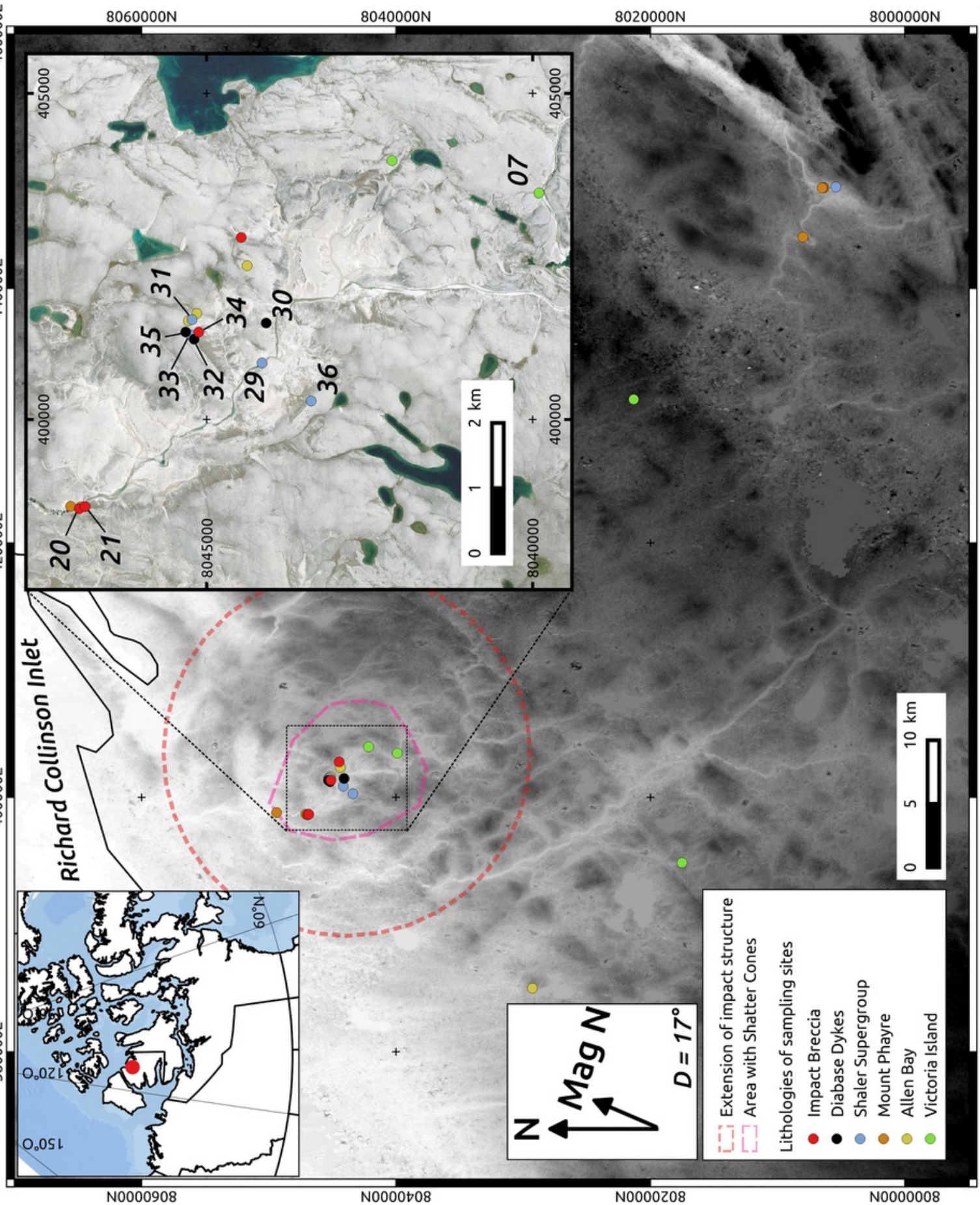
460000E
440000E
420000E
400000E
380000E
8060000N
8040000N
8020000N
8000000N
405000
400000
8045000
8040000
20
21
31
35
33
32
34
29
30
36
07
0 1 2 km
Richard Collinson Inlet
0 5 10 km
N
Mag N
D = 17°
Extension of impact structure
Area with Shatter Cones
Lithologies of sampling sites
Impact Breccia
Diabase Dykes
Shaler Supergroup
Mount Phayre
Allen Bay
Victoria Island
60°N
120°O
150°O

Figure 1

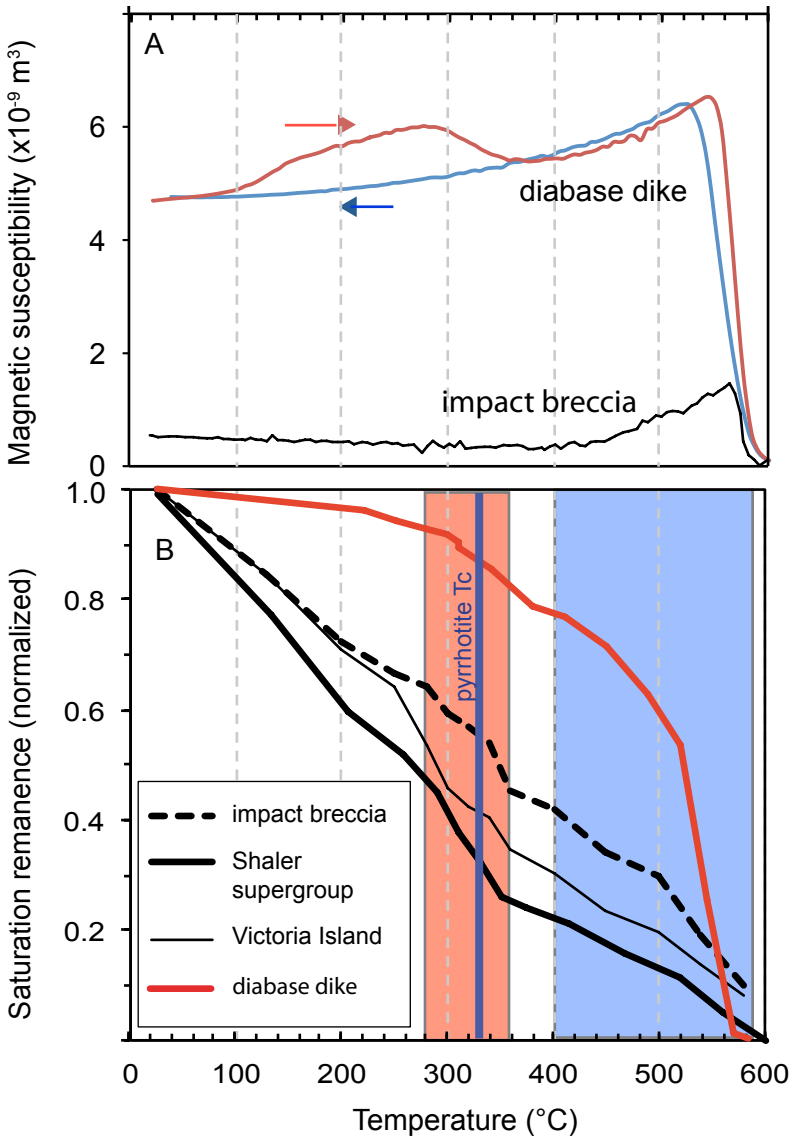
A
Magnetic susceptibility (x10^{-9} m^3)
6
4
2
0
diabase dike
impact breccia
B
Saturation remanence (normalized)
1.0
0.8
0.6
0.4
0.2
pyrrhotite Tc
impact breccia
Shaler supergroup
Victoria Island
diabase dike
0
100
200
300
400
500
600
Temperature (°C)

Figure 2

a) Lithic impact breccias, AF demagnetization

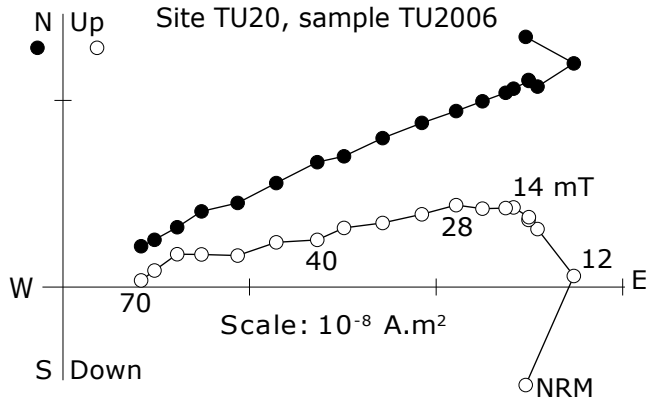

b) Lithic impact breccias, thermal demagnetization

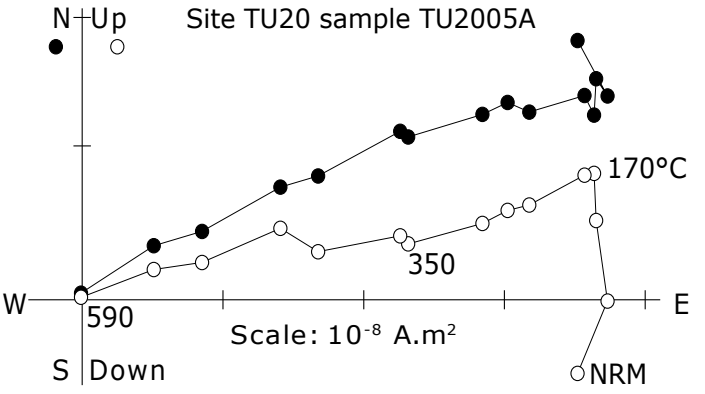

c) Diabase dykes, AF demagnetization

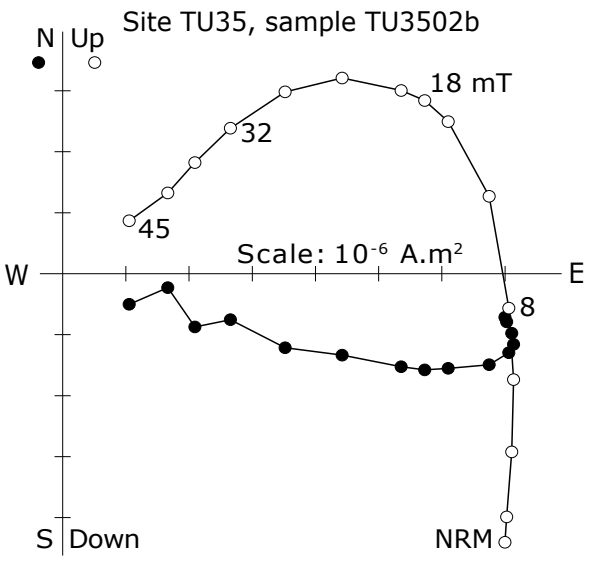

d) Diabase dykes, thermal demagnetization

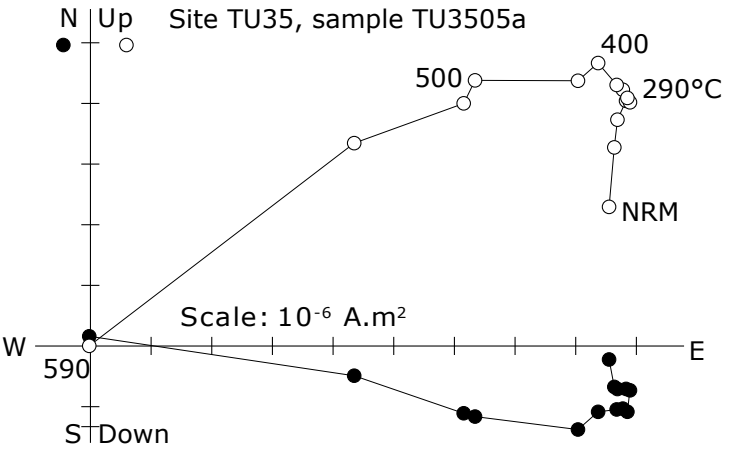

e) Shaler Supergroup sedimentary rocks

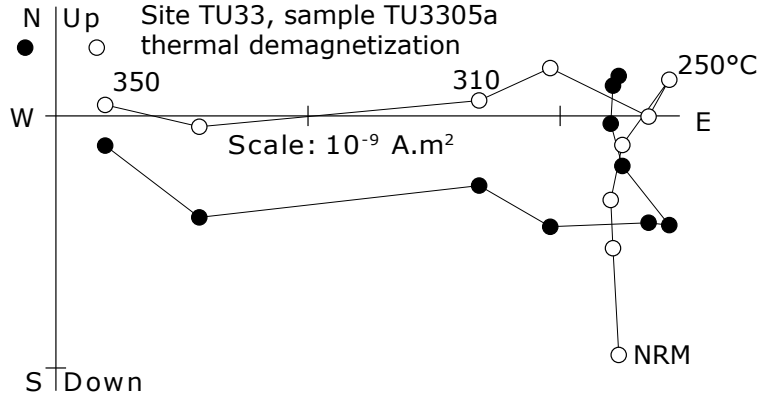

f) Victoria Island sedimentary rocks

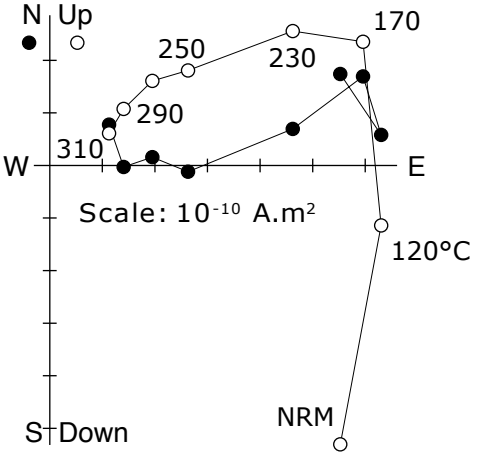

g) Shaler Supergroup sediments baked by diabase dike

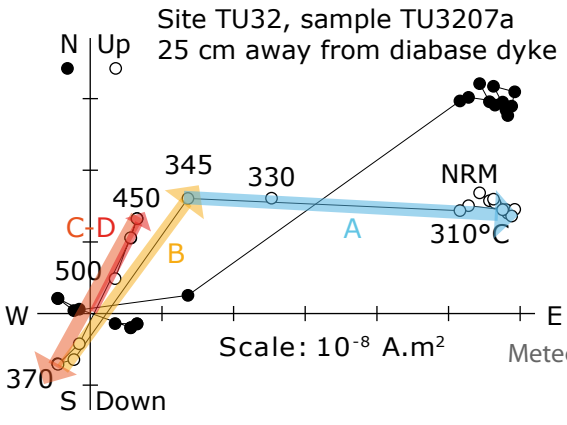

FIGURE 3

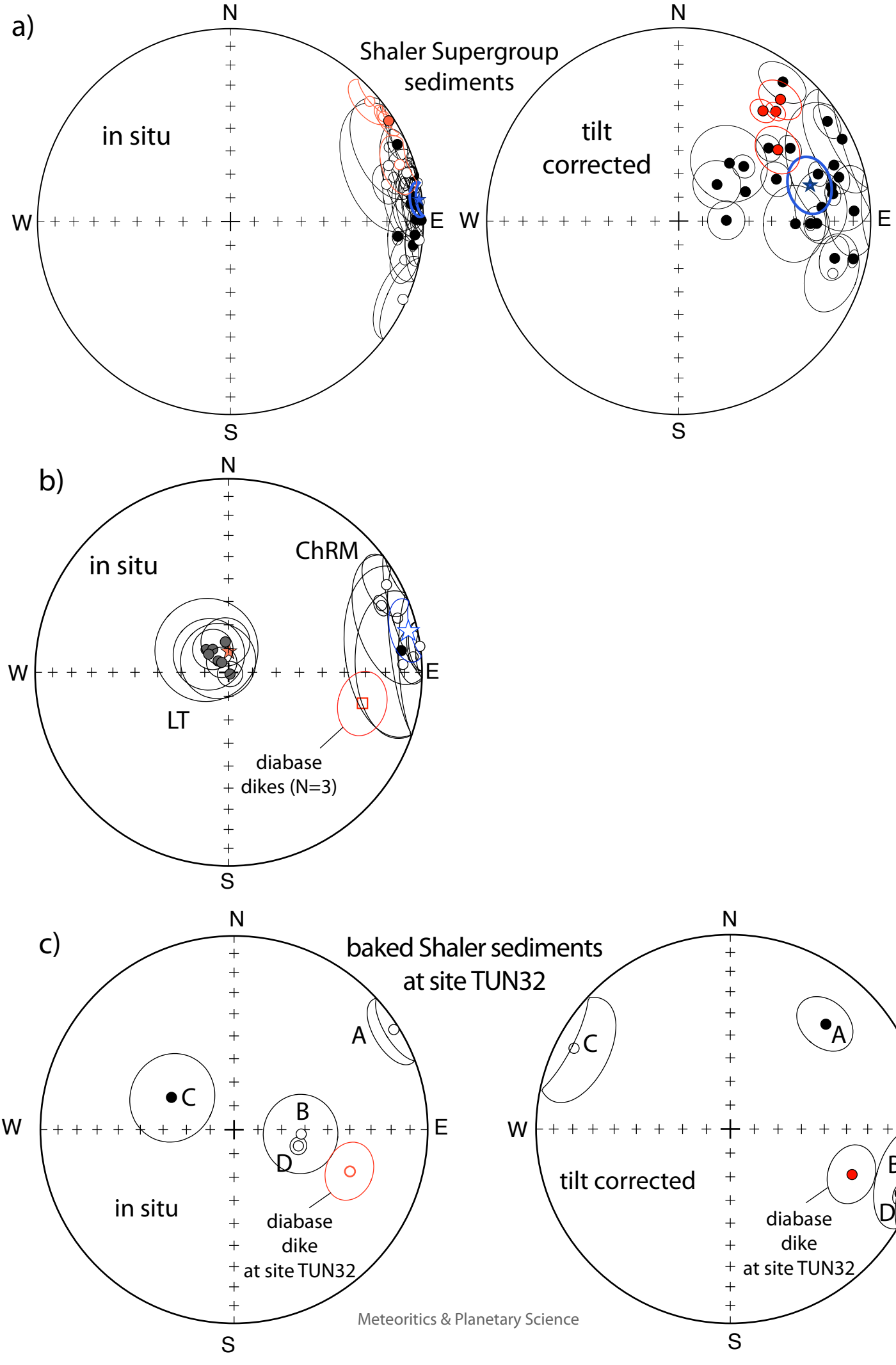
a)
Shaler Supergroup
sediments
in situ
tilt
corrected
N
W
E
S
b)
in situ
ChRM
LT
diabase
dikes (N=3)
c)
baked Shaler sediments
at site TUN32
A
B
C
D
in situ
tilt corrected
diabase
dike
at site TUN32

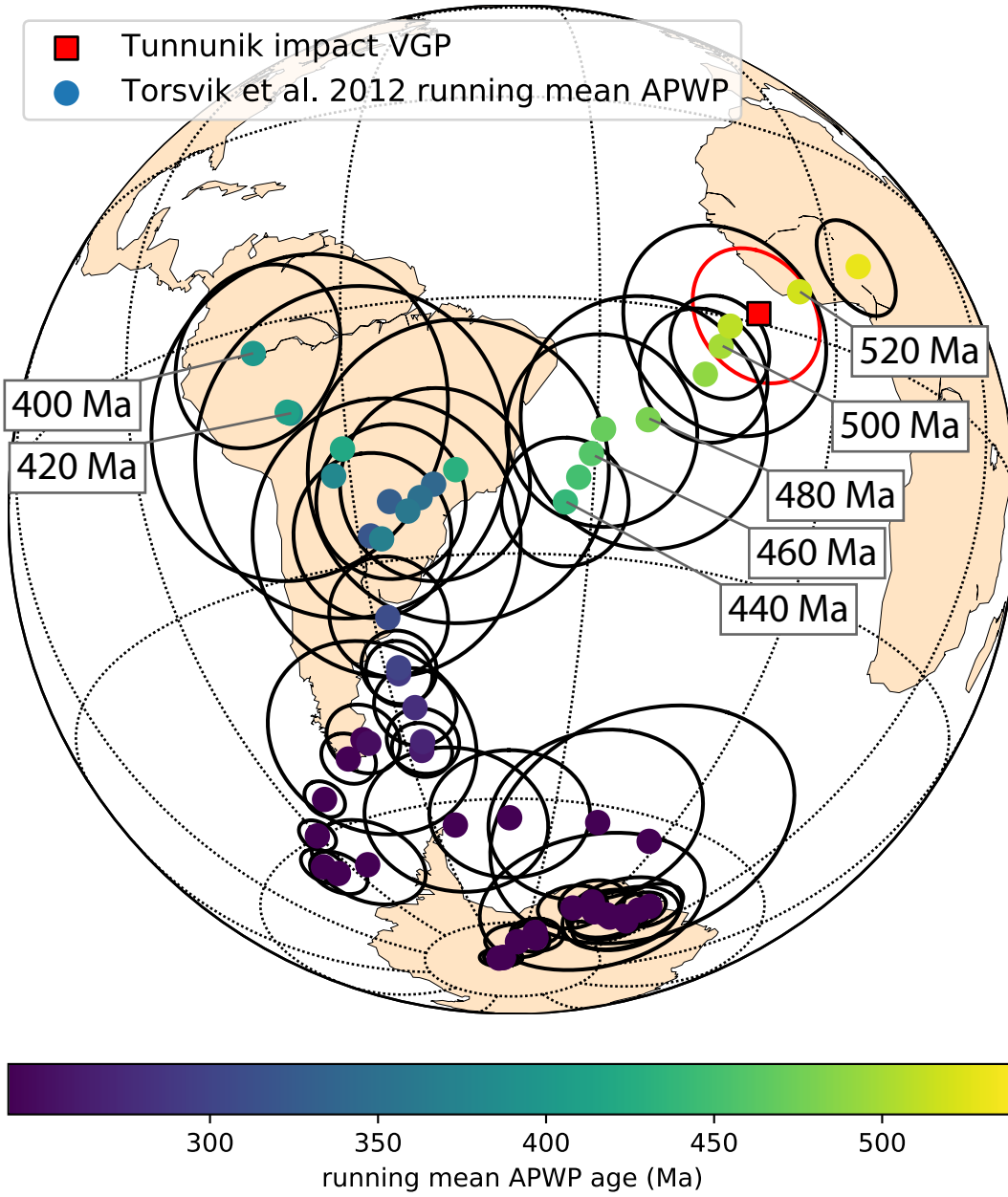
Tunnunik impact VGP
Torsvik et al. 2012 running mean APWP
520 Ma
500 Ma
480 Ma
460 Ma
440 Ma
400 Ma
420 Ma
300
350
400
450
500
running mean APWP age (Ma)

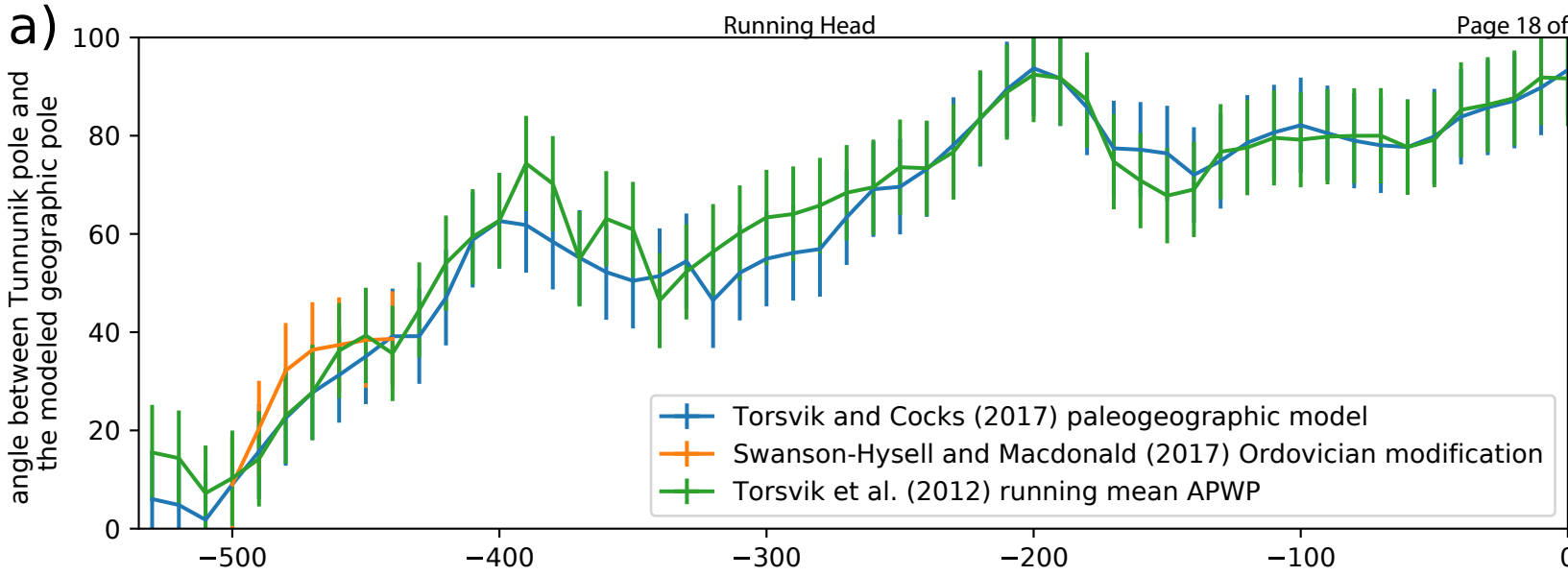
a)
angle between Tunnunik pole and the modeled geographic pole
Torsvik and Cocks (2017) paleogeographic model
Swanson-Hysell and Macdonald (2017) Ordovician modification
Torsvik et al. (2012) running mean APWP

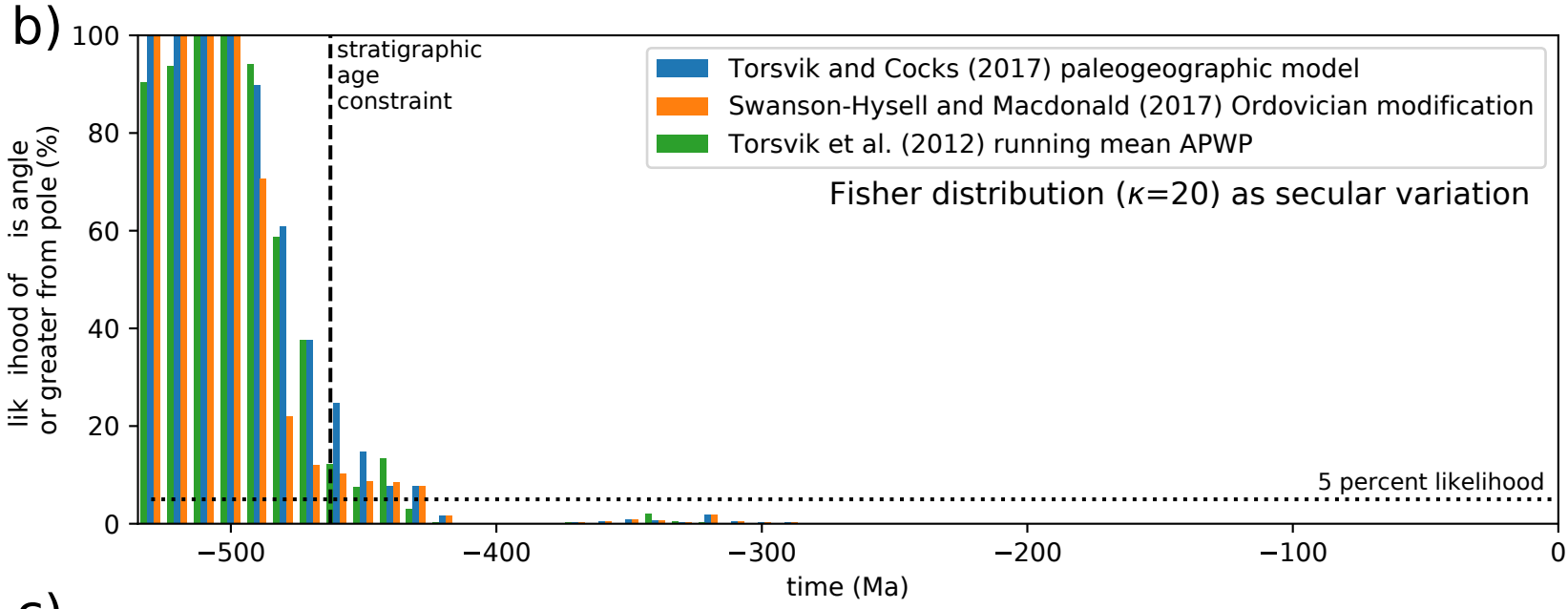
b)
likelihood of angle or greater from pole (%)
stratigraphic age constraint
Torsvik and Cocks (2017) paleogeographic model
Swanson-Hysell and Macdonald (2017) Ordovician modification
Torsvik et al. (2012) running mean APWP
Fisher distribution (κ=20) as secular variation
5 percent likelihood
time (Ma)

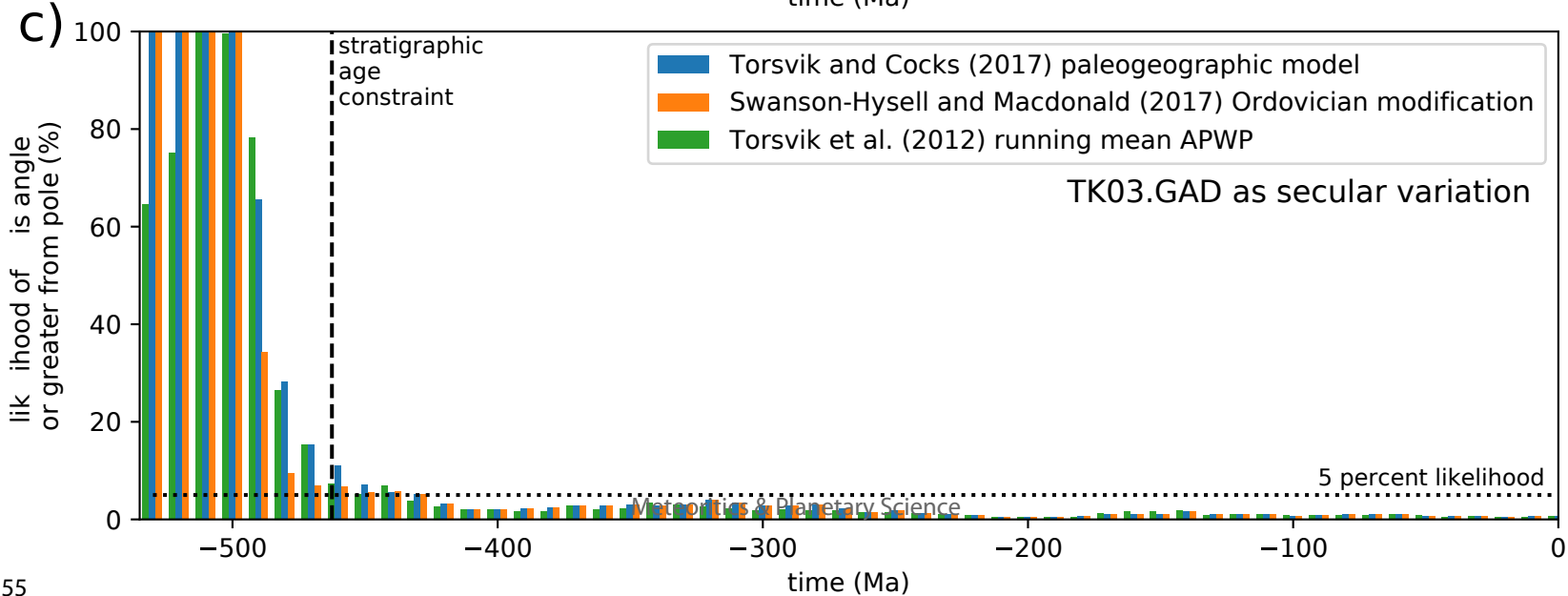
c)
likelihood of angle or greater from pole (%)
stratigraphic age constraint
Torsvik and Cocks (2017) paleogeographic model
Swanson-Hysell and Macdonald (2017) Ordovician modification
Torsvik et al. (2012) running mean APWP
TK03.GAD as secular variation
5 percent likelihood
time (Ma)

Table 1 - Paleomagnetic results

Formation	Site	Slat (°N)	Slong (°E)	N/n	ChRM unblocking temperatures (°C)	D_g (°)	I_g (°)	k_g	$\alpha^{95}{}_g$ (°)	D_s (°)	I_s (°)	k_s	$\alpha^{95}{}_s$ (°)	Strike	Dip	Longg (°)	Latg (°)	dp (°)	dm (°)	Longs (°)	Lats (°)	dp (°)	dm (°)	NRM (Am^2kg^{-1})	χ (m^3kg^{-1})
Impact Breccia	TUN20	72.4973	-114.0209	15/15	260-590	66.6	-15.2	112.5	3.6	66.9	9.5	67.9	4.7	*	*	0.6	-0.6	1.9	3.7	356.9	11.4	2.4	4.7	9.37E-07	6.61E-08
	TUN21	72.4965	-114.0198	5/5	400-530	61.2	-7.8	51.8	10.7	60.8	15.8	51.8	10.7	162	24	4.8	4.6	5.4	10.8	1.9	16.2	5.7	11	5.11E-07	7.39E-08
Victoria Island	TUN07	72.4363	-113.8668	6/9	250-310	83.1	11.2	6.6	28.1	84.3	12.3	6.6	28.1	95	6	34.1	7.5	14.4	28.5	339.7	7.7	14.5	28.6	2.92E-08	-8.21E-10
Shaler Supergroup	TUN29	72.4732	-113.9503	7/7	270-350	85.4	-5.0	52.4	8.4	85.9	22.3	49.9	8.6	170	28	341.2	-1	4.2	8.4	336.5	12.3	4.8	9.1	2.28E-07	1.08E-08
	TUN31	72.4831	-113.9321	5/5	250-350	72.4	-9.3	13.7	21.5	70.6	20.4	13.7	21.5	194	35	354.2	0.7	10.9	21.7	351.6	15.9	11.8	22.5	9.54E-08	1.72E-08
	TUN33	72.4832	-113.9392	9/9	250-330	82.5	-0.5	50.1	7.3	53.8	46.6	11.1	16.2	*	*	343.3	2	3.7	7.3	2.7	37.1	13.4	20.8	1.32E-07	9.35E-09
	TUN36	72.4662	-113.9665	6/6	230-330	87.6	-10.9	8.7	24.0	81.4	-8.0	8.7	24.0	89	36	340	-4.5	12.3	24.3	345.5	-1.3	12.2	24.2	5.43E-08	2.10E-08
Average impact direction*				7/7		77	-5.5	37.2	10	72.7	17.2	16.8	15.2			349.3	1.2	Kg=53.3	A95g=8.3	350.3	14.3	Ks=27,9	A95s=11.6		
baked Shaler Supergroup	TUN32#-A	72.4827	-113.9410	4/4	200-345	58.6	-3.1	67.3	11.3	42.1	28.3	67.3	11.3	207	70	358.9	55.6	10.7	21.5	14.1	31.3	14.4	24.9	3.99E-06	not measured
	TUN32#-B	72.4827	-113.9410	2/2	345-370	97.3	60.2	190	18.2	297.1	-9.8	190	18.2	207	70	145	47	20.9	27.6	128.7	3.1	9.3	18.4	5.19E-06	not measured
	TUN32#-C	72.4827	-113.9410	4/4	370-450	104.2	-62	654	3.6	111	7.4	654	3.6	207	70	339	-44.9	4.3	5.6	315	-2.6	1.8	3.6	3.99E-06	not measured
	TUN32#-D	72.4827	-113.9410	4/4	450-520	93.8	-61.5	33.3	16.2	106.1	6.4	33.3	16.2	207	70	348.3	-41.4	19.2	24.7	319.8	-1.7	8.2	16.2	3.99E-06	not measured
Diabase dikes	TUN30	72.4729	-113.9320	6/6	465-590	98.4	-32.7	10.8	21.3	98.1	23.2	10.8	21.3	184	56	333.6	-19.5	13.6	24.1	324.8	9.1	12	22.7	2.75E-04	1.14E-05
	TUN32	72.4827	-113.9410	5/6	500-590	110	-35.9	48	11.2	110.2	33.7	48	11.2	207	70	323.1	-24.9	7.5	13	311.5	11.7	7.3	12.7	1.87E-04	9.30E-06
	TUN35	72.4839	-113.9379	8/8	500-590	102.3	-29.6	18.5	13.2	101.5	32.8	18.5	13.2	213	66	329.3	-18.8	8.1	14.6	319.8	12.9	8.4	14.9	2.72E-04	1.62E-05
Average diabase dikes				3/3		103.5	-32.8	194	8.9	103.1	29.6	108.8	11.9			328.7	-21.1	Kg=187	A95g=9	318.7	11.3	Ks=140	A95s=10,5		

Meteoritic & Planetary Science

Supporting Information for

A Paleozoic age for the Tunnunik impact structure

Camille Lepaulard[1], Jérôme Gattacceca[1], Nicholas Swanson-Hysell[2], Yoann Quesnel[1], François Demory[1] , Gordon Osinski[3,4],

[1]Aix Marseille Univ, CNRS, IRD, Coll France, INRA, CEREGE, Aix-en-Provence, France

[2] Department of Earth and Planetary Science, University of California, Berkeley, California 94720-4767, USA

[3] Dept. of Earth Sciences, Centre for Planetary Science and Exploration, University of Western Ontario, 1151 Richmond St., London, ON, N6A 5B7, Canada

[4] Dept. Physics & Astronomy, University of Western Ontario, 1151 Richmond St., London, ON, N6A 5B7, Canada

Corresponding author: Camille Lepaulard (lepaulard@cerege.fr)

Contents of this file

Tables S1

Introduction

This supporting information provides an additional table (Table S1).

Formation	Site	Slat (°N)	Slong (°E)	I/O crater	distance from center (km)	paleomagnetic result
Impact Breccia	TUN20	72.4973	-114.0209	Inside	3.3	yes
	TUN21	72.4965	-114.0198	Inside	3.3	yes
	TUN34	72.4821	-113.9376	Inside	0.5	no
	TUN58	72.4769	-113.8936	Inside	3	no
Mafic dikes	TUN12	72.1422	-112.51387	Outside	61	yes
	TUN30	72.4729	-113.9320	Inside	0.7	yes
	TUN32	72.4827	-113.9410	Inside	0.5	yes
	TUN35	72.4839	-113.9379	Inside	0.7	yes
Allen Bay	TUN17	72.3326	-114.39646	Outside	22.6	no
	TUN50	72.4836	-113.93269	Outside	14.9	no
	TUN51	72.4825	-113.9292	Outside	15.2	no
	TUN56	72.4759	-113.9063	Outside	12.3	no
Clastic unit of Mount Phayre formation	TUN14	72.1503	-112.5226	Outside	6	no
	TUN15	72.1513	-112.5230	Outside	61	no
	TUN16	72.1516	-112.52317	Outside	61	no
Shaler Supergroup	TUN13	72.1420	-112.5206	Outside	61	no
	TUN29	72.4732	-113.9503	Inside	0.6	yes
	TUN31	72.4831	-113.9321	Inside	0.7	yes
	TUN33	72.4832	-113.9392	Inside	0.5	yes
	TUN36	72.4662	-113.9665	Inside	1.6	yes
Stripy unit of Mount Phayre formation	TUN21	72.4966	-114.0198	Inside	3.3	no
	TUN22	72.4971	-114.0200	Inside	3.4	no
	TUN23	72.4985	-114.0200	Inside	3.6	no
	TUN28	72.5192	-114.01946	Inside	5.3	no
Tan dolostone unit of Mount Phayre formation	TUN11	72.1643	-112.6376	Outside	56	no
Victoria Island	TUN03	72.4567	-113.85526	Inside	3.8	no
	TUN07	72.4363	-113.8668	Inside	5.2	yes
	TUN10	72.2800	-113.02338	Outside	38	no
	TUN18	72.2321	-114.08812	Outside	28	no

Table S1 - list of sampled sites. Site TUN12 is from a 150 m wide mafic dike located 60 km away from the impact structure. It paleomagnetic direction (D=58°, I=-4°, a95=8.4, k=84, n=5) is different from the three diabase dykes sampled in the impact structure, but this can be easily accounted for by secular variation of the geomagnetic field since the emplacements of these dykes are not necessarily strictly coeval.